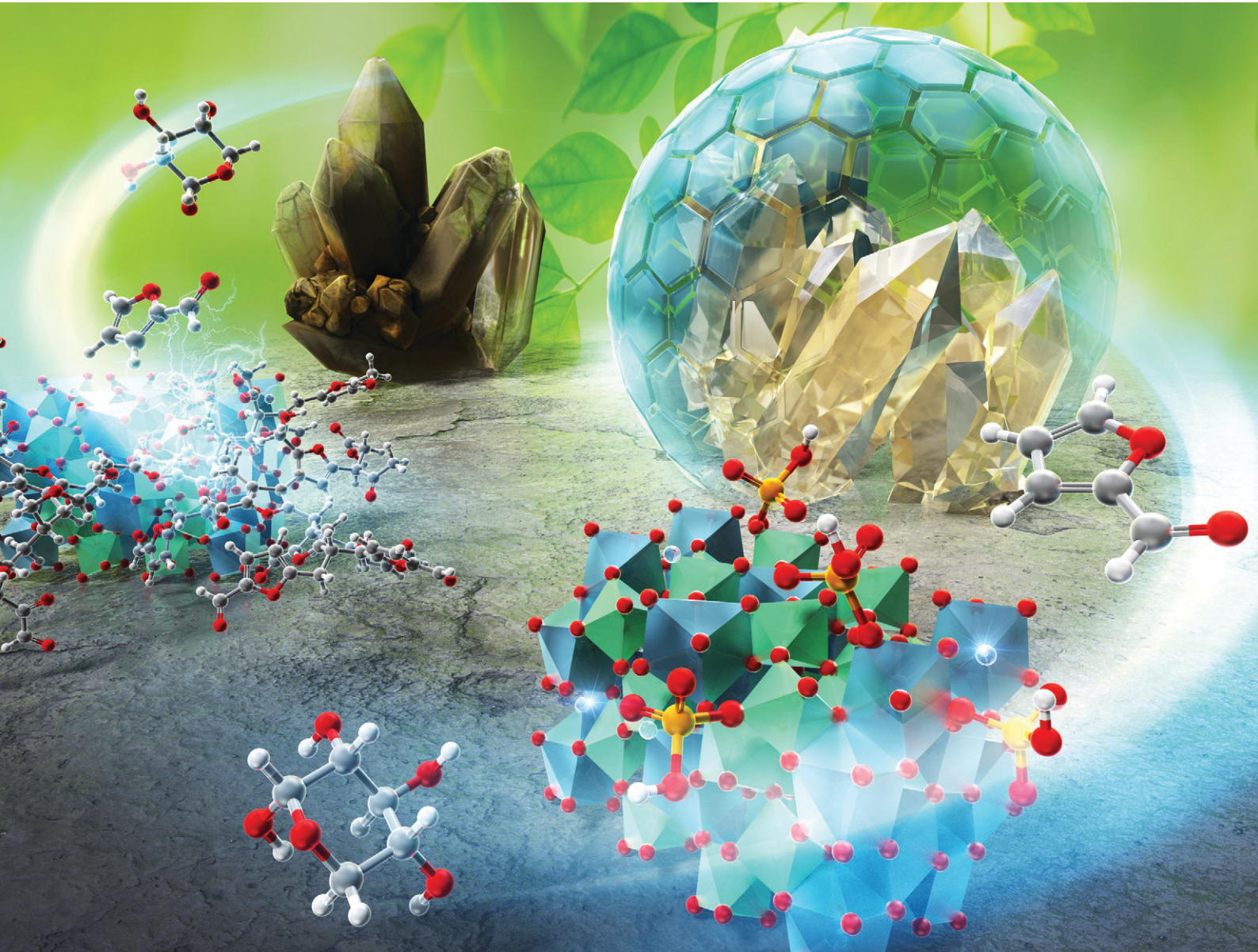


# Catalysis Science & Technology

[rsc.li/catalysis](http://rsc.li/catalysis)



ISSN 2044-4761

## COMMUNICATION

Kiyotaka Nakajima *et al.*  
Lewis acid catalysis of phosphate-modified  $\text{CaNb}_2\text{O}_6$  for  
xylose dehydration to furfural



Cite this: *Catal. Sci. Technol.*, 2025, 15, 2665

Received 4th January 2025,  
Accepted 9th March 2025

DOI: 10.1039/d5cy00010f

rsc.li/catalysis

Phosphate-modified  $\text{CaNb}_2\text{O}_6$  was prepared using the amorphous metal complex method and tested as a solid catalyst for xylose dehydration to furfural. The orthorhombic  $\text{CaNb}_2\text{O}_6$  consists of octahedral  $\text{NbO}_6$  and square antiprismatic  $\text{CaO}_8$ , providing unique Lewis and Brønsted acid sites. These active sites exhibited a higher furfural yield compared to orthorhombic  $\text{Nb}_2\text{O}_5$ .

The effective use of biomass-derived sugars, such as glucose and xylose, as renewable carbon resources can contribute to achieving carbon neutrality.<sup>1</sup> Xylose is a pentose sugar obtained *via* acid-catalyzed hydrolysis of xylan, the main component of hemicellulose.<sup>2</sup> The dehydration of xylose yields furfural, which is reported as one of the top-listed biobased products by the US Department of Energy due to its high potential applications as a green solvent, fuel additive, organic fertilizer, and valuable biopolymer precursor.<sup>3</sup> Previously, we demonstrated that the water-tolerant Lewis acid catalysis of amorphous  $\text{Nb}_2\text{O}_5$  is effective for xylose dehydration, with unsaturated coordination  $\text{Nb}^{5+}$  centers serving as pivotal active sites.<sup>4</sup> However, catalyst reusability remains a significant challenge.<sup>5</sup> In catalytic sugar conversion, insoluble polymers, called humin, are usually formed *via* the polymerization of the substrate, intermediates, and/or products. These by-products are deposited on the surface, leading to severe deactivation. Catalyst regeneration requires calcination ( $>500$  °C) in the presence of oxygen to remove organic deposits, which induces the crystallization of amorphous  $\text{Nb}_2\text{O}_5$ , thereby reducing its intrinsic activity by a decrease in the number of unsaturated  $\text{Nb}^{5+}$  centers, *i.e.*, catalytic active sites.<sup>6</sup> To overcome such thermal instability, it is essential to develop a crystalline Nb-based metal oxide catalyst

that retains its activity even after the thermal post-treatment. The incorporation of additional elements into  $\text{Nb}_2\text{O}_5$  to form Nb-based complex oxides changes its Lewis acidity and enhances its catalytic performance.<sup>6b,c</sup> Similarly, phosphate treatment (P-treatment) effectively tunes catalyst surface properties.<sup>4a</sup> Here, we report the catalysis of  $\text{CaNb}_2\text{O}_6$ , an alkaline earth metal niobate, for xylose dehydration. Orthorhombic  $\text{CaNb}_2\text{O}_6$  consists of octahedral  $\text{NbO}_6$  and square antiprismatic  $\text{CaO}_8$  with edge-sharing structure, while orthorhombic  $\text{Nb}_2\text{O}_5$  features edge-shared  $\text{NbO}_6$  and pentagonal bipyramidal  $\text{NbO}_7$  (Fig. 1). We hypothesized that the unstable edge-sharing structure of  $\text{CaNb}_2\text{O}_6$  facilitates the formation of coordinatively unsaturated Lewis acid sites, enhancing the activity in xylose dehydration. Such a structural future is specific to  $\text{CaNb}_2\text{O}_6$  compared to other alkaline earth metal niobates. The effects of phosphoric acid treatment (P-treatment) on crystalline  $\text{Nb}_2\text{O}_5$  and  $\text{CaNb}_2\text{O}_6$  were also examined to improve their activity.

The amorphous metal complex (AMC) method using a water-soluble niobium peroxy complex was employed to prepare high surface area catalysts.<sup>7</sup> The P-treatment was performed by the procedure reported in our previous papers using a 1 M  $\text{H}_3\text{PO}_4$

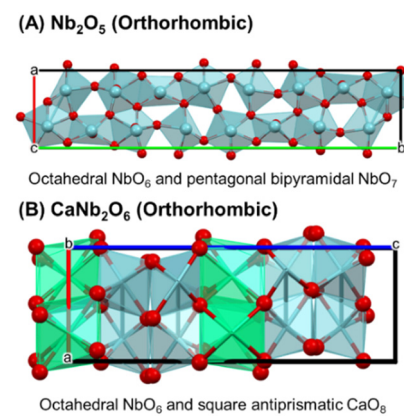


Fig. 1 Crystalline structures of (A)  $\text{Nb}_2\text{O}_5$  and (B)  $\text{CaNb}_2\text{O}_6$ . Red balls, blue and green sticks represent O, Nb and Ca, respectively.

<sup>a</sup> Institute for Catalysis, Hokkaido University, Kita 21 Nishi 10, Kita-ku, Sapporo, Hokkaido 001-0021, Japan. E-mail: nakajima@cat.hokudai.ac.jp

<sup>b</sup> Graduate School of Chemical Sciences and Engineering, Hokkaido University, Kita 13 Nishi 8, Kita-ku, Sapporo, Hokkaido 060-8628, Japan

<sup>c</sup> Institute of Multidisciplinary Research for Advanced Materials, Tohoku University, 2-1-1 Katahira, Aoba-ku, Sendai, 980-8577, Japan

† Electronic supplementary information (ESI) available: Experimental and characterization data. See DOI: <https://doi.org/10.1039/d5cy00010f>

‡ These authors contributed equally.



Table 1 Surface properties of prepared catalysts

Catalysts	$S_{\text{BET}}^a$ ( $\text{m}^2 \text{ g}^{-1}$ )	Surface P content <sup>b</sup> (atom%)	$\text{LAS}^c$ ( $\mu\text{mol g}^{-1}$ )	$\text{BAS}^d$ ( $\mu\text{mol g}^{-1}$ )
$\text{Nb}_2\text{O}_5$	9	—	23	n.d.
$\text{P-Nb}_2\text{O}_5$	9	3.9	14	n.d.
$\text{CaNb}_2\text{O}_6$	23	—	32	<10
$\text{P-CaNb}_2\text{O}_6$	23	2.6	37	10

<sup>a</sup> Determined by  $\text{N}_2$  adsorption. <sup>b</sup> Determined by XPS. <sup>c</sup> Lewis acid site estimated by FTIR measurement of pyridine-adsorbed sample.

<sup>d</sup> Brønsted acid site estimated by FTIR measurement of pyridine-adsorbed sample.

aqueous solution.<sup>4a</sup> The detailed synthetic procedures are described in ESI†.

X-ray diffraction (XRD) measurements (Fig. S1, ESI†) revealed that the orthorhombic phases of both  $\text{CaNb}_2\text{O}_6$  and  $\text{Nb}_2\text{O}_5$  are retained after P-treatment.  $\text{N}_2$  adsorption-desorption measurements (Table 1) showed that  $\text{CaNb}_2\text{O}_6$  has a larger Brunauer–Emmett–Teller (BET) surface area than  $\text{Nb}_2\text{O}_5$ , likely due to the incorporation of the light Ca element. The P contents of the catalysts were estimated using an X-ray photoelectron spectroscopy (XPS) (Fig. S2, ESI†) as 3.9 atom% for  $\text{P-Nb}_2\text{O}_5$  and 2.6 atom% for  $\text{P-CaNb}_2\text{O}_6$  (Table 1).

The acid properties of the catalysts were characterized by *in situ* infrared (IR) spectroscopy with pyridine as a basic probe molecule to quantify Brønsted acid site (BAS) and Lewis acid site (LAS).<sup>8</sup> Fig. 2(A) displays the difference IR spectra of adsorbed pyridine species on  $\text{Nb}_2\text{O}_5$  and  $\text{CaNb}_2\text{O}_6$  before and after P-treatment (see ESI† Fig. S3 for O–H and C–H stretching vibrations). Both  $\text{Nb}_2\text{O}_5$  and  $\text{P-Nb}_2\text{O}_5$  have two specific bands at 1605 and 1444  $\text{cm}^{-1}$  corresponding to typical vibrational modes of the pyridine coordinated on LAS. The P-treatment for  $\text{Nb}_2\text{O}_5$  reduced LAS density (Table 1), indicating that phosphate species deactivate some LASs (Fig. 2(B)). The active LAS of amorphous  $\text{Nb}_2\text{O}_5$  has been proposed as the tetrahedrally coordinated  $\text{NbO}_4$  species in our previous study,<sup>4a,b</sup> and they are fully stabilized with

weakly coordinated and exchangeable  $\text{H}_2\text{O}$  ligand(s). The active LAS of crystalline  $\text{Nb}_2\text{O}_5$  is likely associated with the octahedrally coordinated but oxygen-defective  $\text{NbO}_6$ , and a portion of these LASs lose their Lewis acidity upon the reaction with phosphoric acid. In contrast,  $\text{CaNb}_2\text{O}_6$  has two apparent differences compared to  $\text{Nb}_2\text{O}_5$ : 1) variations in band frequency around 1600  $\text{cm}^{-1}$  and 2) the presence of BAS. Two distinct bands were observed at 1608 and 1602  $\text{cm}^{-1}$  for  $\text{CaNb}_2\text{O}_6$  and  $\text{P-CaNb}_2\text{O}_6$ , which are well-known vibrational modes sensitive to metal type, coordination environment, and acid strength.<sup>8b,9</sup> For instance, the vibrational frequency of adsorbed pyridine on octahedrally coordinated  $\text{AlO}_6$  species in  $\gamma\text{-Al}_2\text{O}_3$  appears at a lower frequency than that of tetrahedrally coordinated  $\text{AlO}_4$  species.<sup>10</sup> In the case of  $\text{CaNb}_2\text{O}_6$ , differences in the coordination environment between defects in  $\text{Nb}-\text{O}-\text{Nb}$  and in  $\text{Nb}-\text{O}-\text{Ca}$  suggest that the two observed bands can be assignable to distinct LASs. Since the vibrational band for liquid-phase pyridine is present at 1580  $\text{cm}^{-1}$ , the higher frequencies observed for  $\text{CaNb}_2\text{O}_6$  indicate stronger interactions, *i.e.*, stronger LASs. Consequently,  $\text{CaNb}_2\text{O}_6$  has both slightly stronger and weaker LASs compared to  $\text{Nb}_2\text{O}_5$ . According to Pauling's principles, the edge-sharing structure is less stable than the corner-sharing structure, leading to a preferential formation of defect sites at  $\text{Nb}-\text{O}-\text{Ca}$  bonds.

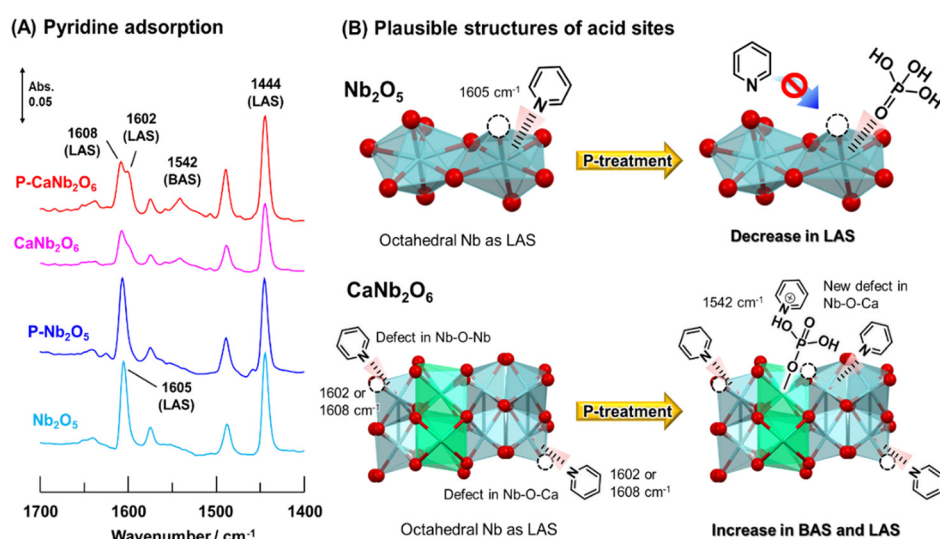


Fig. 2 (A) Difference IR spectra of adsorbed pyridine species on the prepared catalysts at 30 °C. (B) Plausible structures of acid sites on  $\text{Nb}_2\text{O}_5$  and  $\text{CaNb}_2\text{O}_6$  before and after P-treatment. White circles in (B) indicate oxygen defect sites.



Another notable difference is the presence of BAS in  $\text{CaNb}_2\text{O}_6$  and  $\text{P-CaNb}_2\text{O}_6$ . A weak band at  $1542\text{ cm}^{-1}$ , assignable to the vibrational mode of the pyridinium cation,<sup>8</sup> was observed in  $\text{CaNb}_2\text{O}_6$  and became pronounced in  $\text{P-CaNb}_2\text{O}_6$ . The numbers of BASs are summarized in Table 1. The Brønsted acidic nature of  $\text{CaNb}_2\text{O}_6$  probably originate from the polarized Nb–O–Ca bond, where a proton is formed on a negatively charged oxygen atom to satisfy charge compensation. Still, the amount of BAS is negligibly small. P-treatment enhances the hydrolysis of polarized Nb–O–Ca bonds, resulting in the formation of  $\text{Ca-O-PO(OH)}_2$  species and unsaturated coordination Nb sites, as illustrated in Fig. 2(B). The process explains the increase in BASs, which can be attributed to the immobilization of phosphate species. The formation of LAS can be supported by the increased band intensity at  $1602\text{ cm}^{-1}$ . The unsaturated coordination Nb species formed by P-treatment are stabilized with weakly coordinated and exchangeable  $\text{H}_2\text{O}$  ligand(s) and serve as LASs in acid-catalyzed reactions.

The catalytic performance of  $\text{Nb}_2\text{O}_5$  and  $\text{CaNb}_2\text{O}_6$  was evaluated in the dehydration of xylose (Fig. 3(A)). While  $\text{CaNb}_2\text{O}_6$  showed almost the same furfural yield as  $\text{Nb}_2\text{O}_5$ , its furfural selectivity was low. This low furfural selectivity indicates the formation of polymerized by-product so-called humin, which is most likely catalyzed by relatively stronger LASs derived from the octahedrally coordinated  $\text{Nb}^{5+}$  centers in  $\text{CaNb}_2\text{O}_6$ . The P-treatment improved the catalytic performance of both  $\text{CaNb}_2\text{O}_6$  and  $\text{Nb}_2\text{O}_5$ . Notably,  $\text{P-CaNb}_2\text{O}_6$  exhibited higher furfural yield and selectivity compared to the parent  $\text{CaNb}_2\text{O}_6$ , even at almost the same levels of xylose conversion. This improvement suggests an increased rate of

furfural formation accompanied by a decreased rate of humin formation. On the contrary,  $\text{P-Nb}_2\text{O}_5$  showed enhanced furfural selectivity without a significant increase in furfural yield. This behavior suggests that the LAS responsible for humin formation is deactivated by the formation of phosphate moieties on the surface. The effect of P-treatment on crystalline  $\text{Nb}_2\text{O}_5$  was consistent with that observed for amorphous  $\text{Nb}_2\text{O}_5$ , but the enhanced activity of  $\text{CaNb}_2\text{O}_6$  after P-treatment cannot be explained by the deactivation of LAS that causes side reactions.

Our previous study on amorphous  $\text{Nb}_2\text{O}_5$  revealed that LAS produces furfural through the stepwise dehydration of xylose, and intrinsic BAS does not participate in furfural formation (Fig. S4, ESI†).<sup>4a</sup> Assuming that crystalline  $\text{Nb}_2\text{O}_5$  and  $\text{CaNb}_2\text{O}_6$  follow the same reaction pathway, the high activity of  $\text{P-CaNb}_2\text{O}_6$  is unlikely to result from the increased BAS after the P-treatment. Instead, the improved furfural selectivity of  $\text{CaNb}_2\text{O}_6$  is primarily interpreted by the decrease of LAS that causes humin formation. In addition, the increased furfural yield is mainly attributed to an increase in LAS effective for furfural formation (Table 1). We speculate the increase in both LAS and BAS to the hydrolysis of polar  $\text{Ca-O-Nb}$  bond generating phosphate-based BAS and Nb-based LAS during the P-treatment (Fig. 2B). The effect of phosphate loading on the activity of the resulting  $\text{P-CaNb}_2\text{O}_6$  revealed that phosphate species immobilized *via* the equilibrium adsorption method are essential for enhancing the acid properties and improving the catalytic activity (Table 1 and Fig. S5, ESI†).

Control reactions were performed using reference catalysts to confirm the unique catalysis of  $\text{P-CaNb}_2\text{O}_6$ . A mixture of

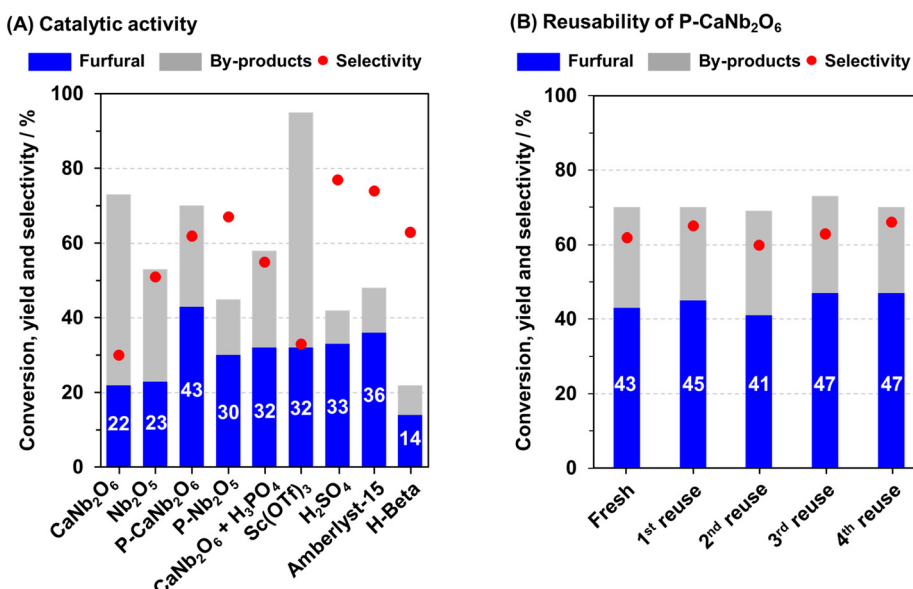


**Fig. 3** (A) Catalytic activity of various catalysts for xylose conversion. Reaction conditions: xylose, 75 mg; catalyst, 300 mg; toluene, 8 mL; water, 2 mL; temperature,  $120\text{ }^\circ\text{C}$ ; time, 5 h. 0.01 mol% of  $\text{H}_3\text{PO}_4$ , 80 mol% of  $\text{H}_2\text{SO}_4$ , and 20 mol% of  $\text{Sc(OTf)}_3$  to substrate were used for the reaction. (B) Reusability test of  $\text{P-CaNb}_2\text{O}_6$ . Reaction conditions are the same as Fig. 3(A). Reused catalysts were calcined at  $500\text{ }^\circ\text{C}$  for 5 h in air before each reaction. Gray bars represent total yield of undetectable by-products including humin. The sum of the blue and gray bars means the xylose conversion.



$\text{CaNb}_2\text{O}_6$  and  $\text{H}_3\text{PO}_4$  improves the target product yield compared to  $\text{CaNb}_2\text{O}_6$  alone. However, the product yield remained lower than that of  $\text{P-CaNb}_2\text{O}_6$ , which evidences that the catalysis of  $\text{P-CaNb}_2\text{O}_6$  is not merely derived from the simple combination of  $\text{CaNb}_2\text{O}_6$  and  $\text{H}_3\text{PO}_4$ .  $\text{P-CaNb}_2\text{O}_6$  demonstrated a higher furfural yield than conventional homogeneous Lewis acid catalyst,  $\text{Sc}(\text{OTf})_3$ . Since Brønsted acid catalysts are known for high furfural selectivity,<sup>11</sup> we compared the catalytic activity of typical homogeneous and heterogeneous Brønsted acid catalysts, such as  $\text{H}_2\text{SO}_4$ , a sulfonated polystyrene resin (Amberlyst-15) and H-beta zeolite. Although the selectivity of  $\text{P-CaNb}_2\text{O}_6$  was slightly lower than that of these Brønsted acid catalysts, it still showed a higher furfural yield, highlighting its great potential as a solid acid catalyst for xylose dehydration. The time-course experiments (Fig. S6, ESI†) showed no significant difference in furfural selectivity between the two catalysts during the reaction, but the reaction rate for furfural formation with  $\text{P-CaNb}_2\text{O}_6$  was larger than that with  $\text{P-Nb}_2\text{O}_5$ , likely due to the large amounts of LAS. Hot filtration experiments (Fig. S7, ESI†) indicate that the reaction completely stopped after the catalyst was removed, implying no obvious leaching of phosphate species during the reaction.

The reusability of heterogeneous catalysts is crucial for industrial applications and serves as a key indicator of catalyst performance. Amorphous  $\text{Nb}_2\text{O}_5$  ( $\text{Nb}_2\text{O}_5\text{-am}$ ) is a promising catalyst for xylose dehydration. To highlight the advantages of crystalline material, the reusability of  $\text{Nb}_2\text{O}_5\text{-am}$  and  $\text{P-CaNb}_2\text{O}_6$  was evaluated. Prior to the reusability test, thermogravimetric-differential thermal analysis (TG-DTA) of fresh and spent  $\text{P-CaNb}_2\text{O}_6$  was performed to determine the optimal regeneration temperature (Fig. S8, ESI†). Continuous weight loss was detected up to 500 °C in the spent catalyst, accompanied by a slight exothermic peak due to the deposited humin species, while there was almost no weight loss in the fresh catalyst. Therefore, the spent catalyst was calcined at 500 °C for 5 h in air to remove the organic deposits before reuse.  $\text{Nb}_2\text{O}_5\text{-am}$  decreased steeply its original activity for the first and second reuse tests (Fig. S9, ESI†). This deactivation is caused by the crystallization of amorphous  $\text{Nb}_2\text{O}_5$  phase during the calcination process, because the strong acidity of  $\text{Nb}_2\text{O}_5\text{-am}$  is derived from its amorphous nature.<sup>6b</sup> The calcination treatment of  $\text{Nb}_2\text{O}_5\text{-am}$  formed orthorhombic  $\text{Nb}_2\text{O}_5$  (Fig. S10, ESI†) and also decreased BET surface area from 120 to 67  $\text{m}^2 \text{ g}^{-1}$ . In contrast,  $\text{P-CaNb}_2\text{O}_6$  retained its original activity even after five cycles (Fig. 3B). XRD measurements revealed no difference between fresh and spent  $\text{P-CaNb}_2\text{O}_6$  (Fig. S11, ESI†), evidencing its high thermal stability towards during regeneration treatment.

## Conclusions

Orthorhombic  $\text{P-CaNb}_2\text{O}_6$  has proven to be an effective catalyst for the conversion of xylose to furfural. *In situ* IR spectroscopy using pyridine as a molecular probe revealed the presence of abundant and stronger LAS on  $\text{P-CaNb}_2\text{O}_6$ .

Such specific surface acidity leads to its better catalytic performance.  $\text{P-CaNb}_2\text{O}_6$  demonstrated excellent reusability for at least five cycles. The choice of the elements and the addition of functions through appropriate post-treatment can be an important factor in the catalytic application of crystalline metal oxides. This approach offers promising opportunities for designing efficient and durable metal oxide catalysts tailored for specific reactions.

## Data availability

The data supporting this article have been included as part of the ESI.†

## Author contributions

Z. W. and K. E. carried out experiments on the synthesis and characterization of catalysts, catalytic reactions. D. P. and H. K. synthesized catalysts. Z. W. wrote the manuscript. R. O., H. K., and K. N. analysed experimental data. R. O., S. S., A. F., H. K., and K. N. revised the manuscript. K. N. supervised the project. All authors provided critical feedback and contributed to the final manuscript.

## Conflicts of interest

There are no conflicts to declare.

## Acknowledgements

This work was supported financially by the following grants: JST-MIRAI Program (Grant number JPMJMI19E3), JST e-Asia Joint Research Program (JPMJSC22E3), JST-PRESTO (JPMJPR2472), JSPS Grant-in-Aid for Transformative Research Areas (A) “Hyper-Ordered Structures Science” (20H05879), JSPS Grant-in-Aid Scientific Research (B) (22H01861), JSPS Grant-in-Aid for Early-Career Scientist (24K17555), the Cooperative Research Program of Institute for Catalysis, Hokkaido University (24ES0579), and the Cooperative Research Program of “Network Joint Research Center for Materials and Devices” (20241118).

## Notes and references

- 1 K. J. Yong, T. Y. Wu, C. B. T. L. Lee, Z. J. Lee, Q. Liu, J. M. Jahim, Q. Zhou and L. Zhang, *Biomass Bioenergy*, 2022, **161**, 106458.
- 2 (a) P. Mäki-Arvela, T. Salmi, B. Holmbom, S. Willför and D. Y. Murzin, *Chem. Rev.*, 2011, **111**, 5638; (b) D. S. Naidu, S. P. Hlangothi and M. J. John, *Carbohydr. Polym.*, 2018, **179**, 28.
- 3 (a) J. J. Bozell and G. R. Petersen, *Green Chem.*, 2010, **12**, 539; (b) K. Yan, G. Wu, T. Lafleur and C. Jarvis, *Renewable Sustainable Energy Rev.*, 2014, **38**, 663; (c) C. B. T. L. Lee and T. Y. Wu, *Renewable Sustainable Energy Rev.*, 2021, **137**, 110172; (d) Z. Zhang and G. W. Huber, *Chem. Soc. Rev.*, 2018, **47**, 1351.

4 (a) N. K. Gupta, A. Fukuoka and K. Nakajima, *ACS Catal.*, 2017, **7**, 2430; (b) K. Nakajima, Y. Baba, R. Noma, M. Kitano, J. N. Kondo, S. Hayashi and M. Hara, *J. Am. Chem. Soc.*, 2011, **133**, 4224; (c) K. Nakajima, R. Noma, M. Kitano and M. Hara, *J. Mol. Catal. A: Chem.*, 2014, **388–389**, 100.

5 (a) K. Nakajima, R. Noma, M. Kitano and M. Hara, *J. Phys. Chem. C*, 2013, **117**, 16028; (b) R. Noma, K. Nakajima, K. Kamata, M. Kitano, S. Hayashi and M. Hara, *J. Phys. Chem. C*, 2015, **119**, 17117; (c) S. M. A. H. Siddiki, Md. N. Rashed, Md. A. Ali, T. Toyao, P. Hirunsit, M. Ehara and K. Shimizu, *ChemCatChem*, 2019, **11**, 383.

6 (a) M. Yang, S. Li and J. Huang, *ACS Appl. Mater. Interfaces*, 2021, **13**, 39501; (b) D. Padovan, K. Endo, T. Matsumoto, T. Yokoi, A. Fukuoka, H. Kato and K. Nakajima, *Small Struct.*, 2023, **4**, 2200224; (c) M. Kim, S. Ronchetti, B. Onida, N. Ichikuni, A. Fukuoka, H. Kato and K. Nakajima, *ChemCatChem*, 2020, **12**, 350.

7 (a) D. Dey, V. Petrykin, S. Sasaki and M. Kakihana, *J. Ceram. Soc. Jpn.*, 2007, **115**, 808; (b) M. Kakihana, M. Kobayashi, K. Tomita and V. Petrykin, *Bull. Chem. Soc. Jpn.*, 2010, **83**, 1285.

8 (a) M. Tamura, K. Shimizu and A. Satsuma, *Appl. Catal., A*, 2012, **433–434**, 135; (b) M. I. Zaki, M. A. Hasan, F. A. Al-Sagheer and L. Pasupulety, *Colloids Surf., A*, 2001, **190**, 261.

9 (a) G. Busca, *Phys. Chem. Chem. Phys.*, 1999, **1**, 723; (b) A. Travert, A. Vimont, A. Sahibed-Dine, M. Daturi and J.-C. Lavallee, *Appl. Catal., A*, 2006, **307**, 98.

10 T. K. Phung, C. Herrera, M. Á. Larrubia, M. García-Díéguez, E. Finocchio, L. J. Alemany and G. Busca, *Appl. Catal., A*, 2014, **483**, 41.

11 (a) B. M. Matsagar, M. K. Munshi, A. A. Kelkar and P. L. Dhepe, *Catal. Sci. Technol.*, 2015, **5**, 5086; (b) B. M. Matsagar, S. A. Hossain, T. Islam, H. R. Alamri, Z. A. Alothman, Y. Yamauchi, P. L. Dhepe and K. C.-W. Wu, *Sci. Rep.*, 2017, **7**, 13508.

